

COMPUTATIONAL PHYSICS

The Computational Physics Section publishes articles that help students and their instructors learn about the physics and the computational tools used in contemporary research. Most articles will be solicited, but interested authors should email a proposal to the editors of the Section, Jan Tobochnik (jant@kzoo.edu) or Harvey Gould (hgould@clarku.edu). Summarize the physics and the algorithm you wish to include in your submission and how the material would be accessible to advanced undergraduates or beginning graduate students.

A guide to hunting periodic three-body orbits

Milovan Šuvakov^{a)} and V. Dmitrašinović^{b)}

Institute of Physics, Belgrade University, Pregrevica 118, Zemun, P.O. Box 57, 11080 Beograd, Serbia

(Received 6 December 2013; accepted 11 February 2014)

The recent discovery of thirteen new and distinct three-body periodic planar orbits suggests that many more such orbits remain undiscovered. Searches in two-dimensional subspaces of the full four-dimensional space of initial conditions require computing resources that are available to many students, and the required level of computational and numerical expertise is also at the advanced undergraduate level. We discuss the methods for solving the planar three-body equations of motion, as well as some basic strategies and tactics for searches of periodic orbits. Our discussion should allow interested undergraduates to start their own searches. Users can submit new three-body orbits to a wiki-based website. © 2014 American Association of Physics Teachers.

[<http://dx.doi.org/10.1119/1.4867608>]

I. INTRODUCTION

Many present day textbooks on classical mechanics, such as Refs. 1–7, discuss chaotic systems, but only a few discuss the three-body problem. Exceptions include Refs. 2, 5, and 7, which range from a mere mention of the problem⁵ to an entire chapter.² Moreover, only a few topics on the restricted three-body problem have been discussed in this journal.^{8,9} The limited discussions of the problem might be due in part to the widely perceived difficulty of obtaining solutions, before the recent deluge of new periodic solutions.¹⁰ Soon after the publication of Ref. 10 we received many e-mails, showing that, given the initial conditions, it takes little time and effort to reconstruct these solutions.

Unlike periodic two-body motion, periodic solutions of Newton's equations governing the motion of three celestial bodies around their common center of mass are not known analytically for arbitrary initial conditions. After Bruns' work¹¹ in the late 19th century, it has been known that periodic three-body solutions cannot be found analytically, with one famous exception—the Lagrange-Euler orbits.^{12,13} Bruns' result does not imply that periodic orbits do not exist. Finding periodic orbits constitutes one part of the classical three-body problem.

With the advent of computers, numerical solutions have been found that can be classified into two (continuously infinite) families of periodic collisionless three-body solutions: (1) the Broucke-Hadjidemetriou-Henon family,^{14–20} and (2) the Moore-Chenciner-Montgomery-Simo “figure-eight” family.^{21–24} These two, together with the much older Lagrange-Euler family,^{12,13} form the three families of solutions known prior to Ref. 10, which recently increased this number to fifteen. Each of the presently known fifteen families contains infinitely many different orbits that might, but need not be stable, depending on their angular momentum and/or their mass ratios. Only two families, the

Lagrange-Euler and the Broucke-Hadjidemetriou-Henon, have been thoroughly explored with regard to stability, angular momentum, and mass-ratio dependences.

In this paper, we argue that finding new periodic solutions is not too difficult and can be done by interested students. We present instructions on how to set up a periodic orbit “search engine,” as well as several successful examples of search tactics and strategies for the do-it-yourself periodic orbit hunter.

Our prior work has used only standard upper level undergraduate and graduate level textbooks and methods that are freely available. Since then, we have learned of the existence of more specialized treatises, such as Ref. 25, which might be helpful to interested readers, but are not indispensable.

The plan of the article is as follows. In Sec. II, we define the equations of motion to be solved, and discuss numerical algorithms that can be used to solve them. In Sec. III, we present a method for searching for periodic orbits. An identification and classification method for periodic orbits is given in Sec. IV. We then show several examples of periodic orbits in Sec. V and discuss initial conditions that are most likely to yield successful future searches. The Appendix describes a program that helps to classify orbits.

II. EQUATIONS OF MOTION

The differential equations of motion of three bodies in a plane described by the position vectors $\mathbf{r}_i = (x_i, y_i)$ and masses m_i are

$$\ddot{x}_1(t) = \frac{Gm_2[x_2(t) - x_1(t)]}{\left[(x_1(t) - x_2(t))^2 + (y_1(t) - y_2(t))^2\right]^{3/2}} - \frac{Gm_3[x_1(t) - x_3(t)]}{\left[(x_1(t) - x_3(t))^2 + (y_1(t) - y_3(t))^2\right]^{3/2}}, \quad (1)$$

$$\ddot{y}_1(t) = \frac{Gm_2[y_2(t) - y_1(t)]}{\left[(x_1(t) - x_2(t))^2 + (y_1(t) - y_2(t))^2\right]^{3/2}} - \frac{Gm_3[y_1(t) - y_3(t)]}{\left[(x_1(t) - x_3(t))^2 + (y_1(t) - y_3(t))^2\right]^{3/2}}, \quad (2)$$

plus another two pairs of equations with $1 \rightarrow 2 \rightarrow 3$ and $1 \rightarrow 3 \rightarrow 2$. Note that the numerators in Eqs. (1) and (2) go to zero when $\mathbf{r}_i \rightarrow \mathbf{r}_j$; that is, there are singularities in the equations of motion when any pair of bodies collide.

Equations (1) and (2) need to be solved numerically by using Runge-Kutta methods or almost any ordinary differential equation solver. The main restriction on the choice of numerical method stems from the fact that although we are searching for collisionless orbits and formally need not worry about “hitting” a singularity, some periodic orbits pass close to one or more of these singularities, in which case the numerical error increases. This behavior requires a shorter time step, but there may be long sections of the orbit that are far away from singularities where the choice of a longer time step is justified and would substantially speed up the computation. Therefore, adaptive time step methods which allow a variable time step are the best choice for the present problem. Unfortunately, adaptive time step methods usually exhibit energy drift in contrast to symplectic algorithms. However, the latter do not allow straightforward implementation of the adaptive-step feature.²⁶ We have chosen an adaptive step Runge-Kutta-Fehlberg method,^{27,28} although this choice is not obligatory. The adaptivity of the time step has certain drawbacks in the calculation of orbits with a predefined period, as discussed in Sec. III F.

The value of the gravitational constant G used in the computations and the average mass $m = \frac{1}{3} \sum_{i=1}^3 m_i$ can be changed by using simple scaling rules, as discussed in Sec. IV B 1. What cannot be changed by such a rescaling are the mass ratios m_1/m_2 , m_3/m_1 , and m_2/m_3 . These ratios, together with the total energy E and the total angular momentum L , are an essential part of the specification of an orbit. One way to obtain more solutions, which we will consider to be in the same family of solutions, is to change the value(s) of L and/or the mass ratios. In all the numerical calculations we discuss, the masses m_1 , m_2 , m_3 , and the gravitational constant G are set to unity, but we will discuss more general choices, for readers who wish to extend the calculations to unequal masses.

To solve for the evolution of the three two-vectors $(\mathbf{r}_1(t), \mathbf{r}_2(t), \mathbf{r}_3(t))$ and their time derivatives $(\mathbf{p}_1(t), \mathbf{p}_2(t), \mathbf{p}_3(t))$, we need to specify their initial conditions. That is, we need to know six two-vectors, which we denote by the 12-vector

$$\mathbf{X}(t) = (\mathbf{r}_1(t), \mathbf{r}_2(t), \mathbf{r}_3(t), \mathbf{p}_1(t), \mathbf{p}_2(t), \mathbf{p}_3(t)) \quad (3)$$

at the initial time $t=0$.

Absolute periodicity of the solution implies that $\mathbf{X}(t)$ returns to its initial value $\mathbf{X}_0 = \mathbf{X}(0)$ at time $t=T$, where T is the period. There is another kind of periodicity, *relative* periodicity, in which all relative positions and relative velocities return to their initial values, but the orientation in the plane has changed by an overall rotation angle. A solution with relative periodicity can be made absolutely periodic by tuning the angular momentum.

III. SEARCH METHOD FOR PERIODIC ORBITS

A. The return proximity function

The return proximity function $d(\mathbf{X}_0, T_0)$ in phase space is defined as the absolute minimum of the distance from the initial condition by $d(\mathbf{X}_0, T_0) = \min_{t \leq T_0} |\mathbf{X}(t) - \mathbf{X}_0|$, where

$$|\mathbf{X}(t) - \mathbf{X}_0| = \sqrt{\sum_i^3 [\mathbf{r}_i(t) - \mathbf{r}_i(0)]^2 + \sum_i^3 [\mathbf{p}_i(t) - \mathbf{p}_i(0)]^2} \quad (4)$$

is the distance (Euclidean norm) between two 12-vectors in phase space (the Cartesian coordinates and velocities of all three bodies without removing the center-of-mass motion). We define the return time $\tau(\mathbf{X}_0, T_0)$ as the time for which this minimum is reached.²⁹ Searching for periodic solutions with a period T smaller than a parameter T_0 is equivalent to finding zeros of the return proximity function. The initial value of T_0 was taken to be around 100, significantly higher than 6.235, the period of the figure-eight solution. The algorithm for finding zeros of the return proximity function is as follows. For steps (2) and (3), we used the Runge-Kutta-Fehlberg algorithm,^{27,28} but any other adaptive time step integration method can be chosen.

1. Choose an initial condition \mathbf{X}_0 , a maximum period T_0 , and the numerical precision ϵ .³⁰
2. Compute the time step Δt so that the calculation error is less than ϵ .
3. Compute \mathbf{X}_{i+1} from \mathbf{X}_i by integrating the equations of motion.
4. Calculate the distance from the initial condition by linear interpolation:

$$d = \left| (\mathbf{X}_0 - \mathbf{X}_i) - \frac{(\mathbf{X}_{i+1} - \mathbf{X}_i) \cdot (\mathbf{X}_0 - \mathbf{X}_i)}{|\mathbf{X}_{i+1} - \mathbf{X}_i|^2} (\mathbf{X}_{i+1} - \mathbf{X}_i) \right|. \quad (5)$$

5. Initially d will increase from its value $d=0$ at $t=0$. If and when the value of d decreases, we check to see if the value of d is minimal, and if yes, we store this value.
6. Repeat steps (2)–(4) while $t < T_0$.

The result of this procedure is the minimum value of d . If d_{\min} is less than some arbitrary tolerance, we use it as a candidate for a periodic solution. This tolerance was 10^{-4} in our calculations, but can be tuned to improve the results. Note that this tolerance is not the final minimum, because we then apply the gradient descent method, which we will describe later. The value of the tolerance plays the role of an initial filter to select candidate regions in phase space.

B. Three-body variables

Because the return proximity function is a function of twelve variables, it is difficult to systematically vary all twelve initial conditions to find a periodic solution. Thus, it is advisable to eliminate all constants of the motion and reduce the number of variables of the proximity function. We first use the obvious symmetries of the three-body system such as translational symmetry to set the total momentum equal to zero and use rotational invariance. One way to do the latter is by changing the three-body variables to relative (Jacobi) ones.

We next introduce the relative three-body coordinates and the shape sphere. We will use the latter for classifying periodic

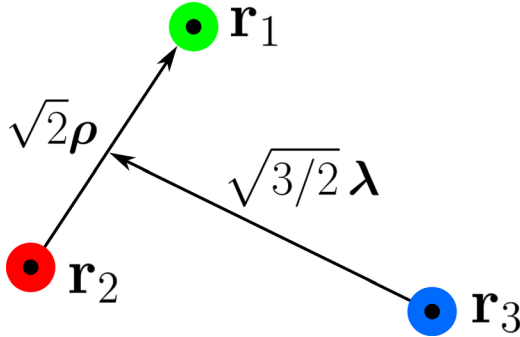


Fig. 1. The two, three-body Jacobi coordinates ρ, λ .

solutions. Because most of these variables remain unchanged for arbitrary masses, we will discuss the general case here.

The center-of-mass (CM) two-vector \mathbf{R}_{CM} is defined for arbitrary masses as

$$\mathbf{R}_{\text{CM}} = \frac{m_1 \mathbf{r}_1 + m_2 \mathbf{r}_2 + m_3 \mathbf{r}_3}{\sum_{i=1}^3 m_i}. \quad (6)$$

\mathbf{R}_{CM} is a constant of the motion if the total linear momentum $\mathbf{P} = m_1 \dot{\mathbf{r}}_1 + m_2 \dot{\mathbf{r}}_2 + m_3 \dot{\mathbf{r}}_3$ equals zero. For this reason, we can reduce the number of variables in the proximity function $d(\mathbf{X}_0, T_0)$ from twelve to eight.

The graphical representation of the three-body dynamics is simplified by using the two relative coordinate vectors introduced by Carl Jacobi³⁶ (see Fig. 1),

$$\rho = \frac{1}{\sqrt{2}}(\mathbf{r}_1 - \mathbf{r}_2) \text{ and } \lambda = \frac{1}{\sqrt{6}}(\mathbf{r}_1 + \mathbf{r}_2 - 2\mathbf{r}_3), \quad (7)$$

which are applicable even for unequal masses. We solve Eqs. (1) and (2) using Cartesian coordinates and then use ρ and λ to graphically represent the solutions. The mass-weighted Jacobi vectors are not necessary for solving the equations of motion, nor do they represent the true geometry of the three-body trajectories. Consequently, they can be avoided altogether.

There are three independent scalar three-body variables: λ^2 , ρ^2 , and $\rho \cdot \lambda$. The hyperradius $R = \sqrt{\rho^2 + \lambda^2}$ characterizes the overall size of the orbit and removes one of the three scalar variables. We may relate the three scalar variables to the unit three-vector $\hat{\mathbf{n}}$ defined by the Cartesian components

$$\hat{\mathbf{n}} = \left(\frac{2\rho \cdot \lambda}{R^2}, \frac{\lambda^2 - \rho^2}{R^2}, \frac{2(\rho \times \lambda) \cdot \mathbf{e}_z}{R^2} \right). \quad (8)$$

The domain of these three-body variables is a sphere with unit radius,^{31,32} as illustrated in Fig. 2. The sphere coordinates depend only on the shape of the triangle formed by the

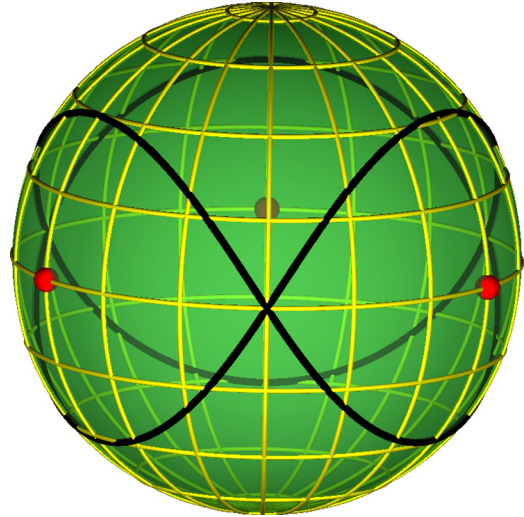


Fig. 2. Figure-eight orbit (solid curve) on the shape-space sphere. Three, two-body collision points (bold), singularities of the potential, lie on the equator.

three bodies, not on R or on its orientation. The equatorial circle corresponds to collinear three-body configurations (degenerate triangles). The three points shown in Fig. 2 correspond to two-body collisions, that is, singularities in the potential. We have constructed an applet³³ that allows users to interactively explore the relation between the shape of the triangle and its position on the shape-space sphere.

Two angles parametrizing the shape sphere together with the hyperradius R define the three-dimensional configuration space of the planar three-body problem. (The total rotation angle can be reconstructed from the trajectory in this space and the condition for angular momentum conservation.) Thus the nominal dimension of phase space is $6 = 3 + 3$, with the three generalized coordinates describing the configuration space and three conjugate generalized momenta. Size or energy scaling reduces the dimension to five. Using the property that “with the exception of Lagrange’s solution, every solution with zero angular momentum to the Newtonian three-body problem suffers syzygies,”^{34,35} we can always choose a collinear configuration for the initial conditions, without losing a potential periodic solution. This second constraint further reduces the dimension of phase space by one, and leaves a four-dimensional space of initial conditions for periodic orbits.

C. Absolute periodic orbits

We can define the reduced return proximity function in phase space as the absolute minimum of the distance from the initial condition by $d(\mathbf{Y}_0, T_0) = \min_{t \leq T_0} |\mathbf{Y}(t) - \mathbf{Y}_0|$, where

$$|\mathbf{Y}(t) - \mathbf{Y}_0| = \sqrt{[\rho(t) - \rho(0)]^2 + [\lambda(t) - \lambda(0)]^2 + [\dot{\rho}(t) - \dot{\rho}(0)]^2 + [\dot{\lambda}(t) - \dot{\lambda}(0)]^2} \quad (9)$$

is the distance between the 8-vector $\mathbf{Y}(t) = (\rho(t), \lambda(t), \dot{\rho}(t), \dot{\lambda}(t))$ and $\mathbf{Y}(0)$. By using these Jacobi relative vectors and velocities, we have removed the center-of-mass motion; that is we have used translational symmetry, but the rotational symmetry remains untreated. The latter can be done as well, but the norm appropriate to that task is no longer Euclidean, and hence we use it only for searches of relative periodic orbits.

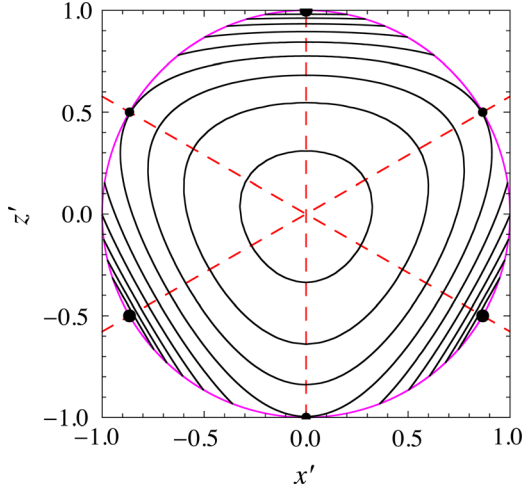


Fig. 3. The equipotential contours for the equal-mass three-body potential (solid) on the shape sphere, as seen from (infinitely) high above the north or south poles. The three straight lines (dashed) correspond to three binary permutations, or transpositions, S_2 subgroups of the full permutation group S_3 . Two rotations by $\phi = \pm 2\pi/3$ about the axis out of the plane of the figure correspond to two cyclic three-body permutations. Note the symmetry of the contours under the reflections about the three transposition lines and the two rotations. Note also the accumulation of contour lines at the two-body collision points (larger solid circles), and the decrease of the density of contours at the three Euler points (smaller solid circles) and the north/south pole.

D. Relative periodic orbits

To eliminate rotational symmetry and thus to search only for relative periodic orbits, we define the 6-vector, $\mathbf{Z}(t) = (x, y, z, \dot{x}, \dot{y}, \dot{z})$, where

$$x = \frac{2\rho \cdot \lambda}{R}, \quad y = \frac{\lambda^2 - \rho^2}{R}, \quad z = \frac{2(\rho \times \lambda) \cdot \mathbf{e}_z}{R} \quad (10)$$

are the shape sphere coordinates multiplied by the hyperradius R . By using the relative return proximity function, $d(\mathbf{Z}_0, T_0) = \min_{t \leq T_0} |\mathbf{Z}(t) - \mathbf{Z}_0|$, in the minimization procedure, we are effectively searching for relative periodic orbits. The six variables in $\mathbf{Z}(t)$ are subject to energy conservation, which reduces its dimension to five, as explained in Sec. III B. The choice of a collinear configuration (a syzygy) for the initial configuration, or equivalently a point on the equator of the shape sphere, forms the second constraint and leaves a four-dimensional “hunting ground” for periodic orbits.

E. Choice of initial conditions

To make the search of the nonlinear four-dimensional space more manageable, we next reduce its dimension by a judicious choice of the initial configuration. A useful tool for doing this reduction is symmetry. For three equal masses, the only remaining symmetry is three-body permutation symmetry—both the kinetic and the potential energies are symmetric under permutations (see Fig. 3). Therefore, it is reasonable to choose an initial configuration that respects the permutation symmetry of the problem: in other words, one that leads to an orbit that has (at least some part of) the same symmetry as the Hamiltonian. A quick look at the known solutions helps to decide how to proceed.

1. The oldest solutions known to us, those due to Lagrange and Euler,^{12,13} correspond to single points on the shape sphere—the north (or south) pole for the Lagrange

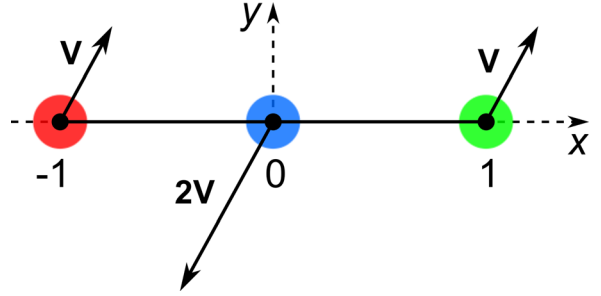


Fig. 4. Initial conditions in the two-dimensional search subspace; symmetric configuration with parallel velocities.

- solution. For the Euler solution it is the Euler point; that is, the intersection of the symmetry meridian and the equator on the shape sphere (see Fig. 3). The Euler point corresponds to a collinear configuration, with one body exactly in the middle between the other two (see Fig. 4). Thus we see that the hyper-angular degree of freedom on the shape sphere is “frozen” in these two orbits and the dynamics is reduced to hyper-radial motion. That is also the reason why these two solutions can be solved in closed form.^{37–39}
2. The second oldest family of solutions, due to Broucke-Hadjidemetriou-Henon,^{14–20} has trajectories in the form of symmetrical ovals on the shape sphere. These ovals have two axes of symmetry: the Euler or symmetry meridian, and the equator, and are centered on one of the two-body collision points. Perusal of Refs. 14, 18–20 shows that these authors used symmetry principles corresponding to our symmetry argument (although they did not use the shape sphere).
 3. The third family contains Moore’s and Simo’s figure-eight solutions, as well as several of their satellites.^{21–24} These solutions have a truly global form on the shape sphere, encircling it twice (see Fig. 2). This family takes into account the full permutation symmetry, and not just one of its two-body subgroups. The initial conditions for both Moore’s and Simo’s figure-eight solutions correspond to one such point—the Euler point.

Thus, perhaps the simplest way of reducing the dimension of the search space is to take a point on one of the three transposition lines in Fig. 3, that is, on one of three symmetry, or Euler meridians on the shape sphere. The most symmetric among them is the Euler point itself. The rest of the initial conditions of Moore’s and Simo’s figure-eight solutions are determined by the condition that the time derivative of the hyperradius vanishes at the initial time $\dot{R}|_{t=0} = 0$ and that the angular momentum vanishes. We will continue to use these two conditions, although they should be relaxed in the future. This use is not to say that this choice is the only potentially useful initial shape, but it has been fruitful so far.

In this subspace of the full initial condition phase space, the three particles’ initial conditions are specified by only two parameters, the initial velocities $\dot{x}_1(0)$ and $\dot{y}_1(0)$. The other initial conditions are given by $x_1(0) = -x_2(0) = 1$, $x_3(0) = 0$, $y_1(0) = y_2(0) = y_3(0) = 0$, $\dot{x}_2(0) = \dot{x}_1(0)$, $\dot{x}_3(0) = -2\dot{x}_1(0)$, $\dot{y}_2(0) = \dot{y}_1(0)$, and $\dot{y}_3(0) = -2\dot{y}_1(0)$. Therefore this two-dimensional subspace can be parameterized with components of the velocity 2-vector ($v_x = \dot{x}_1(0)$, $v_y = \dot{y}_1(0)$) (see Fig. 4). Note that only a limited region of this subspace (the “inside” of the (circular) border curve between the dark and light regions visible in the upper-left-hand corner in Fig. 9) corresponds to negative energies, that is, to bounded motions.

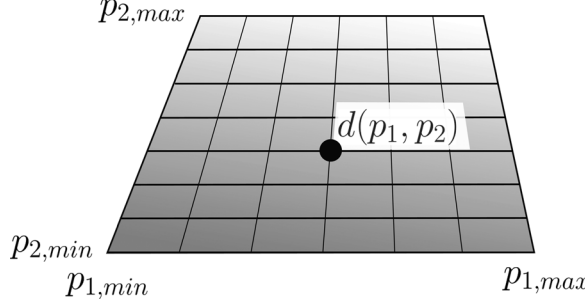


Fig. 5. Discretized search window in the two-dimensional subspace ($p_1 = \dot{x}_1(0)$, $p_2 = \dot{y}_1(0)$) of phase space; $d(p_1, p_2)$ is the return proximity function calculated at each grid point.

F. Direct search for periodic solutions

To look for periodic solutions numerically, we have to discretize the search window in the two-dimensional subspace (see Fig. 5) and calculate the return proximity function for each grid point up to some pre-defined upper limit on the integration time T_0 . In the following we discuss an algorithm for calculating the return proximity function in a window in the search plane.

1. Choose a search window in the search plane parameterized by p_1 and p_2 by fixing the values of $p_{1,\min}, p_{1,\max}, p_{2,\min}, p_{2,\max}$. Choose the grid size (resolution) $N \times M$.
2. For each grid point (i,j) , where $0 \leq i \leq N-1$, and $0 \leq j \leq M-1$, compute the initial condition \mathbf{X}_0 using

$$p_1 = p_{1,\min} + i \frac{p_{1,\max} - p_{1,\min}}{N}, \quad (11)$$

$$p_2 = p_{2,\min} + j \frac{p_{2,\max} - p_{2,\min}}{M}, \quad (12)$$

$$\mathbf{X}_0 = \{1, 0, -1, 0, 0, 0, p_1, p_2, p_1, p_2, -2p_1, -2p_2\}. \quad (13)$$

For this initial condition compute the return proximity d using the algorithm described in Sec. III A.

3. The result of this procedure is an $N \times M$ matrix of return proximity function values in the search window.

For each local minimum of the return proximity function on this grid less than some prescribed tolerance (for example, 10^{-4}), we use the simple gradient descent algorithm⁴⁰ to find the position of the minimum more accurately.

Of course, we cannot *a priori* know for certain if we have missed an orbit within the given period range T_0 , whose orbit's local maximum of the negative logarithm of the return proximity function $-\log d(\mathbf{X}_0, T_0)$ is smaller than the prescribed tolerance on a grid for a given resolution. A miss can be positively determined only after an orbit has been found, usually by increasing the resolution of the search grid.

In the following, we present a gradient descent algorithm which more precisely locates the positions of the minima of the return proximity function in the search plane. The idea of this algorithm is to successively approach the minimum by calculating on an ever smaller-scale 5×5 grid about the candidate point.

1. Fix the time of integration T_0 and the total number of gradient descent steps N_{step} . Choose the initial parameters, $p_{1,0}, p_{2,0}$, and the initial gradient descent resolution, d_p .

2. For each grid point (i,j) , where $-2 \leq i \leq 2$ and $-2 \leq j \leq 2$, compute the initial condition \mathbf{X}_0 using the following:

$$p_1 = p_{1,0} + i d_p, \quad (14)$$

$$p_2 = p_{2,0} + j d_p, \quad (15)$$

$$\mathbf{X}_0 = \{1, 0, -1, 0, 0, 0, p_1, p_2, p_1, p_2, -2p_1, -2p_2\}. \quad (16)$$

3. For each of these initial conditions calculate the return proximity function using the algorithm described in Sec. III A.
4. If the minimum of these 5×5 values is not positioned at the center ($i = 0, j = 0$), then move $p_{1,0}, p_{2,0}$ to the new minimum:

$$p_{1,0} \leftarrow p_{1,0} + i_{\min} d_p, \quad (17)$$

$$p_{2,0} \leftarrow p_{2,0} + j_{\min} d_p, \quad (18)$$

where i_{\min} and j_{\min} are the coordinates of the minimum in the 5×5 matrix.

5. If the minimum of the 5×5 values is positioned at the center ($i = 0, j = 0$), then zoom in to twice the previous resolution: $d_p \leftarrow d_p/2$.
6. Repeat steps (2)–(5) N_{step} times.
7. The result of this procedure is the final position and value of the minimum d .

We have to decide the level of accuracy for the return proximity function d . We used 10^{-6} , but this value can be changed, depending on the required numerical precision.

IV. IDENTIFICATION OF PERIODIC ORBITS

After we have found a periodic orbit, we wish to see if it is new. In the following, we discuss how to identify periodic orbits.

A. Topological identification method

We use the topological identification and classification method for periodic three-body solutions suggested by Montgomery.³² A periodic orbit is a closed curve on the shape sphere. Because we will consider only collisionless periodic orbits, this curve must not pass through any of the three two-body collision points (which are singularities in the potential). Therefore, no such curve can be stretched across any of the two-body collision points without changing its fundamental properties. This condition imposes a constraint on the topology of such curves. The classification problem of closed curves on a sphere with three punctures was solved by mathematicians in the early 20th century, and is given by the conjugacy classes of the fundamental group, which, in this case, is the free group on two letters (a,b) as shown in Fig. 6.

This abstract mathematical notation need not concern the uninitiated because it has a simple geometric interpretation. The idea amounts to classifying closed curves according to their topologies in a plane with two punctures: the sphere can be mapped onto a plane by a stereographic projection using one of the punctures as the north pole (see Fig. 7). This procedure effectively removes one selected puncture to infinity in the plane, and leaves two punctures in the plane.

If we denote a clockwise full turn around the right-hand-side puncture by a, and denote b as the counter-clockwise

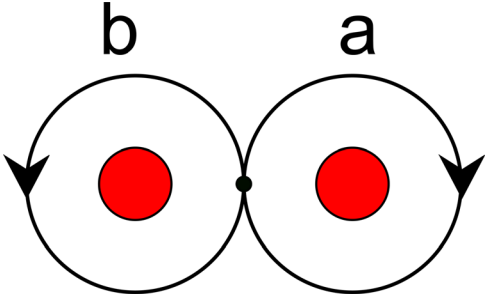


Fig. 6. The two elements (a, b) of the free group.

full turn around the other puncture (see Fig. 6), then every closed curve in such a plane can be described by a sequence of letters a and b , and their inverses $a^{-1} = A$, and $b^{-1} = B$, which we denote by upper case letters. A specific sequence of letters, or word, is not the only descriptor of a specific closed curve (periodic orbit) because there is no preferred starting point of a periodic orbit, and thus any other word that can be obtained by a cyclic permutation of the letters in the original word is an equally good descriptor of such an orbit. The set of all cyclically permuted words is the aforementioned conjugacy class of a free group element (word). For example, the conjugacy class of the free group element aB also contains the word Ba .

Moreover, the time-reversed orbits correspond to physically identical solutions, but their free group elements and their conjugacy classes are generally different. So, for example, families of orbits described by a and A are equivalent, but families ab and AB are not because the inverse of ab is BA , not AB . There is another ambiguity concerning the simplest families of orbits (a and b). As can be seen in Fig. 7 by applying the stereographic projection of the shape sphere onto a plane, a simple loop around the third (“infinite”) puncture on the shape sphere corresponds to aB , a loop around both poles in the plane, but a single loop around any one of the three punctures on the original shape sphere must be equivalent to either of the two remaining punctures; consequently, aB is equivalent to a and b .

The reading of the free group words for new orbits can be done by visually following the orbit and counting the number of times it circles around one or the other preferred puncture in the shape sphere. Take, for example the figure-eight orbit:^{21,22} its trajectory on the shape sphere, Fig. 2 can be distorted as in Fig. 8 and is related to the conjugacy class of the word $abAB$.¹⁰

For illustration purposes, we can make a mechanical model to help with this counting. The model consists of a

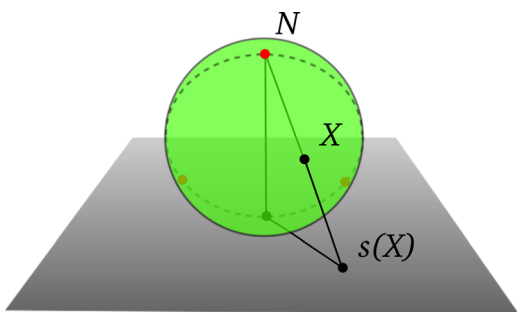


Fig. 7. Sketch of the stereographic projection of a sphere onto a plane. Three, two-body collision points (solid, red online) lie on a meridian (dashed circle), with one of them being at the north pole (denoted by the letter N).

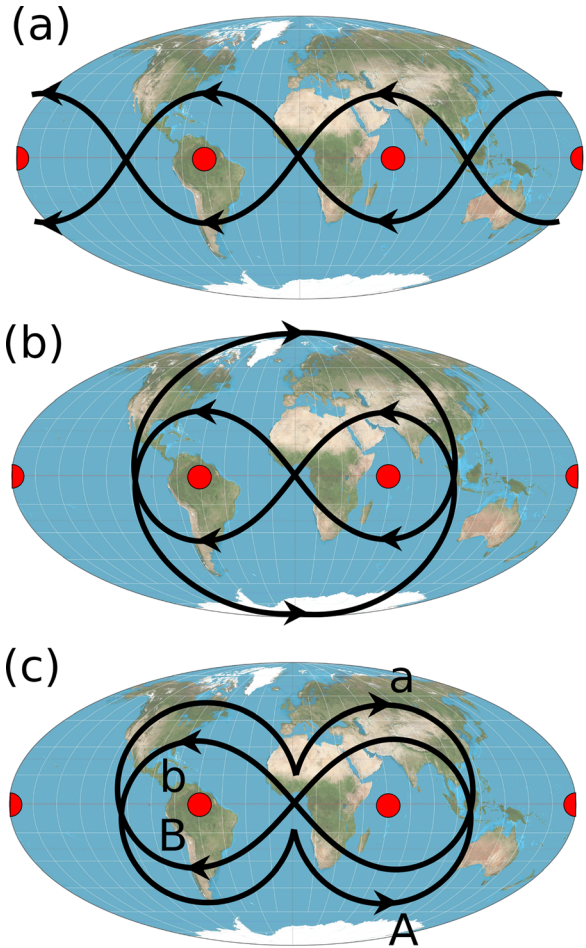


Fig. 8. Three topologically equivalent views of the figure-eight orbit on the shape sphere in Mollweide projection, wherein the third pole on the equator is split into two halves, one of each being displayed at the eastern and the western “end”: (a) the original orbit, as in Fig. 2; (b) a deformed version, wherein the orbit is slid over the North and South poles; (c) the final version, adapted to the reading of the free group element, see Fig. 6.

ping-pong or rubber ball, representing the shape-sphere, with three pins that represent the three collision points on the equator, and a (closed) rubber band that represents the trajectory. We insert the rubber band around the three pins

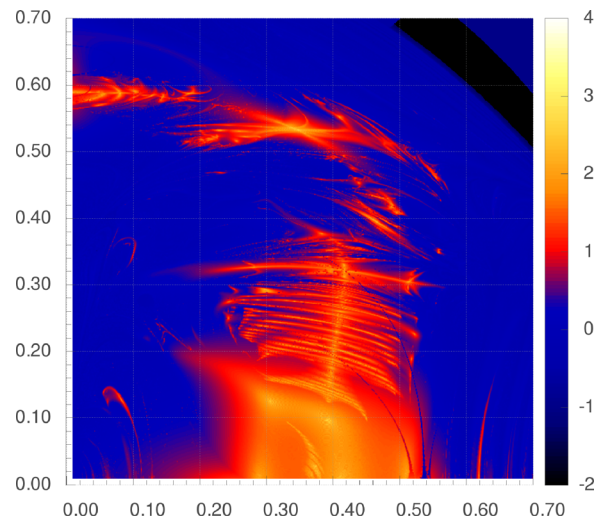


Fig. 9. The negative logarithm of the return proximity function $-\log_{10} d(\mathbf{X}_0, T_0)$ in the (velocity) search plane.

according to the found solution, and then stretch it and/or slide it around until it clings only to two pins. Then we can read off the free group word from the rubber band tangle around the two pins.

This counting can be done easily for sufficiently short and simple orbits, but the method quickly becomes tiresome, unreliable, and difficult for long words, such as seen in the lower rows of Table I. For this reason, we have devised a program, described in the Appendix, which reads the free group word from the solution by analyzing the sequence of the equator segments that the trajectory passes in one period. This program is available at the Orbitopedia website.⁴³

The figure-eight orbit^{21,22} is related to the conjugacy class of the word abAB.¹⁰ The figure-eight solution can be described as a slalom; that is, as a motion in a zigzag manner on the shape sphere between the two-body singularities, while drifting in the same general direction along the equator, for example, eastward or westward (see Fig. 2). As a consequence of parity, the number of full turns (the winding number) around the shape sphere sufficient to reach the initial conditions must be even, and the minimal number is two, as is the case for the choreographic figure-eight orbit,²⁴ as well as its non-choreographic cousin found by Simo.²³

Besides periodic solutions with a simple free group word w , consisting of the letters a, b, A, B, that is, $w = w(a, b, A, B)$, there are satellite orbits, which are described by free group words that are integer powers of the original simple word, that is, $w^k = w^k(a, b, A, B)$, where k is an integer. For example, there are orbits that track around the shape sphere's equator (either westward or eastward) $2k$ times, while slaloming between the two-body collision points, before closing the loop. Such curves, with a winding number $2k$, belong to the conjugacy class of the free group element $(abAB)^k$, and are called figure-8 (k) satellites. For specific examples see Sec. V B.

Table I. Initial conditions and periods for periodic three-body orbits.¹⁰ $\dot{x}_1(0), \dot{y}_1(0)$ are the first particle's initial velocities in the x - and y -directions, respectively, and T is the period. The other two particles' initial conditions are specified by two parameters as $x_1(0) = -x_2(0) = -1$, $x_3(0) = 0$, $y_1(0) = y_2(0) = y_3(0) = 0$, $\dot{x}_2(0) = \dot{x}_1(0)$, $\dot{x}_3(0) = -2\dot{x}_1(0)$, $\dot{y}_2(0) = \dot{y}_1(0)$, $\dot{y}_3(0) = -2\dot{y}_1(0)$. The gravitational constant G is taken to be $G = 1$ and $m_{1,2,3} = 1$. All solutions have inversion partners (mirror images) in all four quadrants; that is, if $\dot{x}_1(0), \dot{y}_1(0)$ is a solution, so are $\pm\dot{x}_1(0), \pm\dot{y}_1(0)$. Some of these partners are identical to the originals, others are identical up to time-reversal, and others are related to the originals by a reflection; we consider all of them to be physically equivalent to the originals. Note that two pairs of initial conditions in the same quadrant (II.C.2a and II.C.2b; and II.C.3a and II.C.3b) specify only two independent solutions. See the text for explanation.

Class, no. and name	$\dot{x}_1(0)$	$\dot{y}_1(0)$	T	Free group element
I.A.1 butterfly I	0.306892758965492	0.125506782829762	6.23564136316479	$(ab)^2(ab)^2$
I.A.2 butterfly II	0.392955223941802	0.0975792352080344	7.00390738764014	$(ab)^2(ab)^2$
I.A.3 bumblebee	0.184278506469727	0.587188195800781	63.5345412733264	$(b^2(Abab))^2A^2(babaB)^2ba \times (B^2(abAB)^2a^2(BAba)^2BA)$
I.B.1 moth I	0.464445237398184	0.396059973403921	14.8939113169584	$ba(BAB)ab(ABA)$
I.B.2 moth II	0.439165939331987	0.452967645644678	28.6702783225658	$(abAB)^2A(babaB)^2B$
I.B.3 butterfly III	0.405915588857606	0.230163127422333	13.8657626785699	$(ab)^2(ABA)(ba)^2(BAB)$
I.B.4 moth III	0.383443534851074	0.377363693237305	25.8406180475758	$(babABA)^2a(abaBAB)^2b$
I.B.5 goggles	0.0833000564575194	0.127889282226563	10.4668176954385	$(ab)^2ABBA(ba)^2BAAB$
I.B.6 butterfly IV	0.350112121391296	0.0793394773483276	79.4758748952101	$((ab)^2(ab)^2)^6A((ba)^2(BA)^2)^6B$
I.B.7 dragonfly	0.080584285736084	0.588836087036132	21.2709751966648	$(b^2(AbabAB))(a^2(BAbaBA))$
II.B.1 yarn	0.559064247131347	0.349191558837891	55.5017624421301	$(babABabABA)^3$
II.C.2a yin-yang I	0.513938054919243	0.304736003875733	17.328369755004	$(ab)^2(ABA)ba(BAB)$
II.C.2b yin-yang I	0.282698682308198	0.327208786129952	10.9625630756217	$(ab)^2(ABA)ba(BAB)$
II.C.3a yin-yang II	0.416822143554688	0.33033312988282	55.78982856891	$(abaBAB)^3(abaBABab)(ABAbab)^3(AB)^2$
II.C.3b yin-yang II	0.417342877101898	0.313100116109848	54.2075992141846	$(abaBAB)^3(abaBABab)(ABAbab)^3(AB)^2$

B. Other identification methods

1. Scaling

Two systems of three identical particles with different values of their overall positions and velocities (hence also with different energies) have similar solutions if they can be scaled into each other.⁴¹ To check if two periodic solutions are equivalent up to a scaling of their spatial and temporal coordinates, we let $\mathbf{r} \rightarrow \alpha \mathbf{r}$. Then by Eqs. (1) and (2), we let $t \rightarrow \alpha^{3/2}t$. Consequently, the velocity scales as $\mathbf{v} \rightarrow \mathbf{v}/\sqrt{\alpha}$, the total energy scales as $E \rightarrow \alpha^{-1}E$, and the period T as $T \rightarrow \alpha^{3/2}T$. Hence, the equivalency consists of rescaling the solutions described by the same free group word to the same (total) energy and then checking if their (rescaled) periods are identical. If the answer is no, the two solutions are clearly distinct; if the answer is positive, such as in the case of Moore's and Simo's figure-eights, we must use other methods of distinguishing between them. For example, we may look at some specific point on the shape sphere, such as the Euler point, and test if the orbit passes through it. Or, we may look at the specifics of the hyperradial motion, which distinguishes between the two orbits, as for the case of the two figure-eight solutions.

2. How to recognize a choreography?

Choreographic motions, or choreographies for short, are periodic orbits of few-body systems in which all bodies move along the same trajectory with an equal time delay. For three body systems, the masses follow each other with the time delay $T/3$, where T is the period. Therefore, when we observe a choreographic solution delayed by $T/3$, we see the same motion as without this delay, but with a cyclic permutation of the three particles.⁴² This condition for choreographic motion implies that $\mathbf{X}(t + T/3) = \hat{P}\mathbf{X}(t)$, where \hat{P} is

a cyclic permutation of the three bodies. On the shape sphere the cyclic permutation \hat{P} has a simple representation, which is rotation by $2\pi/3$ around the vertical z -axis. Therefore, the trajectory on the shape sphere is symmetrical under rotation by $2\pi/3$. This fact can be used when making a dedicated search for choreographies. The space of initial conditions can be chosen as before for non-choreographic orbits, but one would have to use the condition $\mathbf{X}(t + T/3) = \hat{P}\mathbf{X}(t)$ as the “filter” instead of the usual periodicity condition $\mathbf{X}(t + T) = \mathbf{X}(t)$ in the definition of the choreographic return proximity function $d_{\text{choreo}}(\mathbf{X}_0, T_0)$.

V. EXAMPLES OF PERIODIC ORBITS

As mentioned in Sec. III E, several periodic orbits have been published in Refs. 14–21 and Ref. 23. Their initial conditions, real-space and shape-space trajectories can be found at Ref. 43. We will not discuss these orbits here, except to mention that Broucke-Hadjidemetriou-Henon family of periodic orbits has recently been extended to include some satellites⁴⁴ using methods similar to the ones described here. That fact makes us believe that, with a small extension of the present methods, further such satellite solutions can be found and explored by readers. Instead of dwelling on these solutions, we will consider more recent solutions.

A. Post-Moore-an orbits

First we summarize the results from Ref. 10. By using course-grained steps in our scan of the velocity search plane (the two-dimensional subspace of the full four-dimensional phase space of initial conditions), we found about 50 different regions containing candidates for periodic orbits, with a return proximity of 10^{-1} in phase space. We then used the gradient descent method⁴⁰ to refine these initial conditions so that the return proximity became less than $<10^{-6}$. We found 15 solutions, 13 of which are distinct, which can be classified into 12 topologically distinct families, as listed in Table I. The reduction of the number of independent orbits occurs because two pairs of initial conditions (yin-yang I and II) specify only two independent solutions, the respective members of the pairs are related by a simple rescaling of space and time, and because two distinct solutions (butterfly I and II) belong to the same topological class.

Both the return proximity function $d(\mathbf{X}_0, T_0)$ and the return time $\tau(\mathbf{X}_0, T_0)$ were calculated. Only the return proximity function is shown in Fig. 9. For each local minimum of the return proximity function less than 10^{-4} (bright dots in Fig. 9) we used the simple gradient descent method on this grid to find the position of the minimum (root) more accurately. All minima below 10^{-6} are listed in Table I and are labeled in Fig. 9.

B. Satellites of the figure-eight orbit

Subsequent to Ref. 10, Šuvakov²⁴ focused his numerical search on a smaller window in the same two-dimensional subspace around the figure-eight initial conditions: $\dot{x}_1(0) \in (0.20, 0.45)$, $\dot{y}_1(0) \in (0.51, 0.56)$, with all other initial values remaining the same as in Ref. 10. The equations of motion were integrated up to time $T_0 = 100$, where the time unit is fixed by the condition that $G = 1 = m_i$, $i = 1, 2, 3$, for each initial condition out of the 125×1000 possibilities (points on the grid) within the search window. The minima of the return

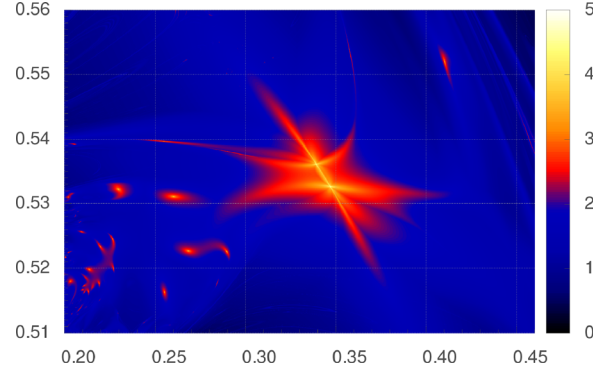


Fig. 10. The logarithm of the reciprocal of the return proximity function $-\log_{10} d(\mathbf{X}_0, T_0)$ in the search window around the initial conditions for the figure-eight solutions in the velocity search plane. The values of the initial velocity $\dot{x}_1(0) \in (0.20, 0.45)$ are on the x -axis and the values of the initial velocity $\dot{y}_1(0) \in (0.51, 0.56)$ are on the y -axis.

proximity function are shown in Fig. 10 and the periodic orbits are tabulated in Table II. The initial conditions for Moore’s figure-eight choreography and Simo’s figure-eight orbit are labeled by F8 and S8, respectively, in Table II. All of these orbits are slaloms of some power k , that is, their topologies are k th powers of the figure-eight orbit (formally their homotopy class is $(abAB)^k$). Such orbits are sometimes called satellites of the figure-eight.

C. Satellites of other known orbits: Promising hunting grounds

Other stable orbits in Table I are likely to have satellites of their own. Table I reveals that the “yarn” solution, II.B.1, is the third power of the “moth I” orbit, I.B.1. Consequently, we expect higher-order satellites of moth I to exist with

Table II. Initial conditions and periods of three-body orbits found by a detailed search in the vicinity of the figure-8 solutions. Here $\dot{x}_1(0)$, $\dot{y}_1(0)$ are the first particle’s initial velocities in the x - and y -directions, respectively, T is the period, and k is the slalom power (that is, $(abAB)^k$ is the homotopy class of the orbit). We also list Moore’s (M8) and Simó’s (S8) figure-eight orbits, for comparison.

Label	$\dot{x}_1(0)$	$\dot{y}_1(0)$	T	k
M8	0.3471128135672417	0.532726851767674	6.3250	1
S8	0.3393928985595663	0.536191205596924	6.2917	1
NC1	0.2554309326049807	0.516385834327506	35.042	7
NC2	0.4103549868164067	0.551985438720704	57.544	7
O1	0.2034916865234370	0.5181128588867190	32.850	7
O2	0.4568108129224680	0.5403305086130216	64.834	7
O3	0.2022171409759519	0.5311040339355467	53.621	11
O4	0.2712627822083244	0.5132559436920279	55.915	11
O5	0.2300043496704103	0.5323028446350102	71.011	14
O6	0.2108318037109371	0.5174100244140625	80.323	17
O7	0.2132731670875545	0.5165434524230961	80.356	17
O8	0.2138543002929687	0.5198665707397461	81.217	17
O9	0.2193730914764402	0.5177814195442197	81.271	17
O10	0.2272123532714848	0.5200484344272606	82.671	17
O11	0.2199766127929685	0.5234338500976567	82.743	17
O12	0.2266987607727048	0.5246235168190009	83.786	17
O13	0.2686383642458915	0.5227270888731481	88.674	17
O14	0.2605047016601568	0.5311685141601564	89.941	17
O15	0.2899041109619139	0.5226240653076171	91.982	17

periods that are longer than 100. This neighborhood is perhaps the most promising for orbit hunting.

Orbits other than moth I may have satellites of their own whose periods are longer than 100, and/or whose orbits do not pass through any of the Euler points, which would explain why they have not yet been found. Each of the 13 recently found orbits should have its neighborhood examined more carefully than has been done so far. To do so means increasing T_0 and making the grid mesh finer, as was done in Ref. 24 for the figure-eight solutions.

We have set up a wiki-based web site,⁴³ Orbitopedia, of three-body orbits, where users can submit newly found orbits and check if they coincide with some previously known orbit.

VI. CONCLUDING REMARKS

We have shown how to hunt numerically for new three-body periodic solutions using readily available computing resources. A map of known solutions, up to period $T = 100$ with masses $m_i = 1$, $i = 1, 2, 3$ and $G = 1$ was shown, together with a detailed map of a smaller area on this map. An increasing number of new solutions is expected to appear as the length of T is extended. Moreover, previously found orbits (may) have satellites of their own that are worth seeking.

We hope to have inspired readers to join us in this search and make a meaningful contribution.

ACKNOWLEDGMENTS

This work was supported by the Serbian Ministry of Education, Science and Technological Development under Grant Nos. OI 171037 and III 41011. The computing cluster Zefram was used extensively for calculations. The authors thank Marija R. Janković for valuable comments.

APPENDIX: THE FREE GROUP WORD READING ALGORITHM

We have devised a program that “reads” the free group word from the periodic solution.

The main idea of this algorithm is to determine the sequence of topologically different syzygies (crossings of different segments of the equator) by following the trajectory on the shape sphere and converting that sequence into a free-group element (word). This conversion is done in two steps: first, we convert the sequence of syzygies into a sequence of directed-semi-circles on the shape sphere using Table III, and illustrated in Fig. 11. We then convert this sequence of directed-semi-circles into a string of free group elements (“letters”) using Table IV. A more detailed description follows.

We assume, for definiteness, that the initial (and therefore also the final) configuration is the syzygy with the second body in the middle (segment 2 (Ref. 46) in Fig. 11). If this assumption is not correct,⁴⁶ we have to apply an appropriate renumbering before proceeding further. The algorithm that determines the free group element for a given solution is as follows:

1. Initialize a list of syzyges ℓ_{syz} with a single element corresponding to the initial configuration: $\ell_{\text{syz}} = \{2\}$. Here $\{2\}$

Table III. Substitution rules for two subsequent entries $(\ell_{\text{syz},i}, \ell_{\text{syz},i+1})$ in the sequence of syzygies into a sequence of directed semi-circles $(\mathcal{A}, \mathcal{B}, \mathcal{C}, \mathcal{D}, \mathcal{E}, \mathcal{F}, \mathcal{G}, \mathcal{H})$. Note the dependence on the parity of the number of equator crossings.

$(\ell_{\text{syz},i}, \ell_{\text{syz},i+1})$	odd i	even i
(12)	\mathcal{F}	\mathcal{D}
(13)	\mathcal{FA}	\mathcal{DG}
(21)	\mathcal{B}	\mathcal{H}
(23)	\mathcal{A}	\mathcal{G}
(31)	\mathcal{EB}	\mathcal{CH}
(32)	\mathcal{E}	\mathcal{C}

means that the initial configuration corresponds to the second segment on the equator.

2. Integrate the equations of motion for given initial conditions (using the same algorithm as in Sec. III A) and at each integration time step compute the mixed product $(\rho \times \lambda) \cdot e_z$ of the Jacobi variables ρ and λ and the out-of-plane unit vector e_z . A passing through a collinear configuration (crossing of the equator on the shape sphere, or a syzygy) is detected when this product changes sign. At each such moment, determine which body is in the middle and put the middle body’s index (number) into the list ℓ_{syz} .
3. After step (2), if the integration time is slightly larger than the period of the solution, the last element in the list ℓ_{syz} should be 2. If it is not, then append it to the list.
4. Convert the list of syzygies ℓ_{syz} to the list of semi-circles ℓ_{hc} as follows. Starting from $i = 1$, for each pair of subsequent elements $(\ell_{\text{syz},i}, \ell_{\text{syz},i+1})$ in the sequence of syzygies append one or two semi-circle labels ($\mathcal{A}, \mathcal{B}, \mathcal{C}, \mathcal{D}, \mathcal{E}, \mathcal{F}, \mathcal{G}$, and \mathcal{H}) to the list ℓ_{hc} according to the rules in Table III.⁴⁵
5. Read off the free-group element of the periodic orbit from the list ℓ_{hc} by substituting two-by-two semi-circle letters according to the rules outlined in Table IV.

We next discuss an example of the implementation of this algorithm to read the free group element of the orbit with a single-loop on the shape sphere. Take a look at Fig. 11 and choose, for definiteness, the loop around the left-hand-side

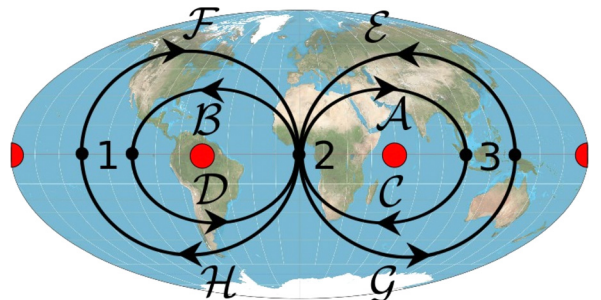


Fig. 11. Illustration of the conversion scheme of a sequence of syzygies (numbered dots on the equator) into a sequence of directed-semi-circles on the shape sphere: eight directed semi-circles connecting different segments of the equator are denoted by the letters $\mathcal{A}, \mathcal{B}, \mathcal{C}, \mathcal{D}, \mathcal{E}, \mathcal{F}, \mathcal{G}$, and \mathcal{H} . The numbers $i = \{1, 2, 3\}$ on each segment denote the index i of the i th body that is placed in the middle of the corresponding collinear configuration (syzygy). We have drawn two dots for each of the two syzygies 1 and 3, for better visibility.

Table IV. Substitution rules for the conversion of a pair of directed semi-circles into one free group element (“letter”).

$(\ell_{hc, 2i-1}, \ell_{hc, 2i})$	
\mathcal{AC}	a
\mathcal{GE}	A
\mathcal{BD}	b
\mathcal{HF}	B

pole. This loop corresponds to the sequence $\{2, 1, 2\}$ of equator crossings, which according to Table III corresponds to the sequence of directed semi-circles \mathcal{BD} , which, in turn, corresponds to the free group letter b, according to Table IV.

Problem. Implement the algorithm to read the free group element of the figure-8 orbit in Fig. 8.

^{a)}Electronic mail: suki@ipb.ac.rs

^{b)}Electronic mail: dmitrasin@ipb.ac.rs

¹J. V. José and E. J. Saletan, *Classical Dynamics: A Contemporary Approach* (Cambridge U.P., Cambridge, 1998), Chap. 7.5.

²D. Hestenes, *New Foundations for Classical Mechanics*, 2nd ed. (Kluwer Academic Publishers, New York, 1999), Sec. 6-5.

³H. Goldstein, C. Poole, and J. Safko, *Classical Mechanics*, 3rd ed. (Addison-Wesley, San Francisco, 2000), Chap. 11.

⁴W. Greiner, *Classical Mechanics: Systems of Particles and Hamiltonian Dynamics* (Springer-Verlag, New York, 2003), Chaps. 21–25.

⁵T. W. B. Kibble and F. H. Berkshire, *Classical Mechanics*, 5th ed. (Imperial College Press, London, 2004), Chap. 14.

⁶F. Scheck, *Classical Mechanics: Systems of Particles and Hamiltonian Dynamics*, 4th ed. (Springer-Verlag, New York, 2005), Chap. 6.

⁷J. M. Finn, *Classical Mechanics* (Infinity Science Press, Hingham, MA, 2008), Chap. 5.4.

⁸James A. Blackburn, M. A. H. Nerenberg, and Y. Beaudoin, “Satellite motion in the vicinity of the triangular libration points,” *Am. J. Phys.* **45**, 1077–1081 (1977).

⁹Richard Greenberg and Donald R. Davis, “Stability at potential maxima: The L_4 and L_5 points of the restricted three-body problem,” *Am. J. Phys.* **46**, 1068–1070 (1978).

¹⁰M. Šuvakov and V. Dmitrašinović, “Three classes of Newtonian three-body planar periodic orbits,” *Phys. Rev. Lett.* **110**, 114301 (2013).

¹¹E. H. Bruns, “Über die Integrale des Vielkörper-Problems,” *Acta Math.* **11**, 25–96 (1887).

¹²J. L. Lagrange, “Essai sur le problème des trois corps,” Oeuvres tome 6; *Miscellanea Taurinensis* **4**, 118–243 (1772); J. L. Lagrange, *Oeuvres*, **2**, pp. 67–121; J. L. Lagrange, *Mécanique Analytique*, pp. 262–286; 2nd ed. **2**, pp. 108–286; J. L. Lagrange, *Oeuvres* **12**, pp. 101–114.

¹³Jean d’Alembert, in a paper of 1761 mentions that Euler had given a method for integrating a certain differential equation “in 1740 (seven years before there was question of the Problem of Three Bodies).” See d’Alembert, “Opuscules Mathématiques,” Vol. 2, Paris 1761, Quatorzième Mémoire (“Réflexions sur le Problème des trois Corps, avec de Nouvelles Tables de la Lune...”) pp. 329–312, at Sec. VI, p. 245. Euler’s original publication is probably L. Euler, Nov. Comm. Acad. Imp. Petropolitanae, **10**, 207–242 ; L. Euler, *ibid.* **11**, 152–184; Mémoires de l’Acad. de Berlin, **11**, 228–249. A more recent textbook dealing with Eulerian solutions is Ref. 37, albeit also without the original reference.

¹⁴R. Broucke and D. Boggs, “Periodic orbits in the planar general three-body problem,” *Celest. Mech.* **11**, 13–38 (1975).

¹⁵J. D. Hadjidemetriou, “The continuation of periodic orbits from the restricted to the general three-body problem,” *Celest. Mech.* **12**, 155–174 (1975).

¹⁶J. D. Hadjidemetriou and Th. Christides, “Families of periodic orbits in the planar three-body problem,” *Celest. Mech.* **12**, 175–187 (1975).

¹⁷J. D. Hadjidemetriou, “The stability of periodic orbits in the three-body problem,” *Celest. Mech.* **12**, 255–276 (1975).

¹⁸R. Broucke, “On relative periodic solutions of the planar general three-body problem,” *Celest. Mech.* **12**, 439–462 (1975).

¹⁹M. Henon, “A family of periodic solutions of the planar three-body problem, and their stability,” *Celest. Mech.* **13**, 267–285 (1976).

²⁰M. Henon, “Stability of interplay motions,” *Celest. Mech.* **15**, 243–261 (1977).

²¹C. Moore, “Braids in classical gravity,” *Phys. Rev. Lett.* **70**, 3675–3679 (1993).

²²A. Chenciner and R. Montgomery, “A remarkable periodic solution of the three-body problem in the case of equal masses,” *Ann. Math.* **152**, 881–901 (2000).

²³C. Simó, “Dynamical properties of the figure eight solution of the three-body problem,” in *Celestial Mechanics*, edited by Alain Chenciner, Richard Cushman, Clark Robinson, and Zhihong Jeff Xia (AMS, Providence, RI, 2002).

²⁴M. Šuvakov, “Numerical search for periodic solutions in the vicinity of the figure-eight orbit: Slaloming around singularities on the shape sphere,” e-print [arXiv:1312.7002](https://arxiv.org/abs/1312.7002).

²⁵B. Leimkuhler and S. Reich, *Simulating Hamiltonian Dynamics* (Cambridge U.P., Cambridge, 2004), Chaps. 1–4.

²⁶A. S. Richardson and J. M. Finn, “Symplectic integrators with adaptive time steps,” e-print [arXiv:1108.0322v1](https://arxiv.org/abs/1108.0322v1).

²⁷Erwin Fehlberg, “Low-order classical Runge-Kutta formulas with step size control and their application to some heat transfer problems,” NASA Technical Report 315 (1969) (unpublished). See also “Klassische Runge-Kutta-Formeln vierter und niedrigerer Ordnung mit Schrittweiten-Kontrolle und ihre Anwendung auf Wärmeleitungsprobleme,” Computing (Arch. Elektron. Rechnen) **6**, 61–71 (1970).

²⁸Ernst Hairer, Syvert Nørsett, and Gerhard Wanner, *Solving Ordinary Differential Equations I: Nonstiff Problems*, 2nd ed. (Springer-Verlag, Berlin, 1993), Chap. II.5.

²⁹More formally $\tau(\mathbf{X}_0, T_0) = \arg \min_{t \leq T_0} |\mathbf{X}(t) - \mathbf{X}_0|$ Here $|\cdot|$ presents the Euclidean norm, but for other purposes (for example, searching for the reduced periodic solution) different metrics can be used.

³⁰The numerical precision ε gives an upper bound of the error, which is defined as the phase-space distance from the numerical value to the exact solution at each time step; we used $\varepsilon = 10^{-15}$ in our computations. General (for example, Cauchy-Peano’s existence) theorems guarantee the existence of an exact solution to the initial value problem (away from the poles). See E. A. Coddington and N. Levinson, *Theory of Ordinary Differential Equations*, (McGraw-Hill, New York, 1955), Chaps. 1–2, or Gerald Teschl, *Ordinary Differential Equations and Dynamical Systems* (Am. Math. Soc., Providence, 2012), Chaps. 2.2–2.5. Numerical analysis provides a piecewise-linear approximation to this exact solution, the convergence of which depends on the approximation method.

³¹T. Iwai, “A geometric setting for internal motions of the quantum three-body system,” *J. Math. Phys.* **28**, 964, 1315–1326 (1987).

³²R. Montgomery, “The N-body problem, the braid group, and action-minimizing periodic solutions,” *Nonlinearity* **11**, 363–376 (1998).

³³The applet is available at suki.ipb.ac.rs/3points/.

³⁴R. Montgomery, “The zero angular momentum, three-body problem: All but one solution has syzygies,” *Ergodic Theor. Dyn. Syst.* **27**(6), 1933–1946 (2007).

³⁵A “syzygy” is a collinear configuration, or equivalently a point on the equator of the shape sphere.

³⁶Carl Gustav Jacob Jacobi, *Vorlesungen über Dynamik, Gesammelte Werke*, Vol. VIII, Supplement (1884); reprinted by (Chelsea Publishing Company, New York, 1969), pp. 221–231.

³⁷L. A. Pars, *Analytical Dynamics* (Heinemann, London, 1965), Chap. XXIX.

³⁸A. Sommerfeld, *Mechanik*, 4th ed. (1949), Chap. 32. Translated into English by Martin O. Stern and published as Mechanics (Academic Press, New York, 1952).

³⁹E. T. Whittaker, *A Treatise on the Analytical Dynamics of Particles and Rigid Bodies, with an Introduction to the Problem of Three Bodies*, 4th ed. (Dover Publications, New York, 1937), Chap. 170.

⁴⁰Jan A. Snyman, *Practical Mathematical Optimization: An Introduction to Basic Optimization Theory and Classical and New Gradient-Based Algorithms* (Springer, New York, 2005).

⁴¹L. D. Landau and E. M. Lifshitz, *Mechanics*, 3rd ed. (Butterworth-Heinemann, Oxford, 1976), Sec. 10.

⁴²Here the first mass is shifted into the position of the second, the second into the third, and the third into the position of the first.

⁴³See supplementary material at <http://dx.doi.org/10.1119/1.4867608> for suki.ipb.ac.rs/3body/, for Orbitopedia, www.orbitopedia.org/.

⁴⁴Marija R. Janković and Milovan Šuvakov, “Extension of the Broucke-Hadjidemetriou-Henon family of periodic orbits in the Newtonian planar three-body problem,” manuscript in preparation.

⁴⁵We assume, without loss of generality, that the trajectory initially lies above the equator (see Fig. 11) and follows one of the upper directed semi-circles described by one of the caligraphic letters $\{\mathcal{A}, \mathcal{B}, \mathcal{E}, \mathcal{F}\}$. At each equator crossing the subset of caligraphic letters that describe the trajectory changes from the “upper” subset $\{\mathcal{A}, \mathcal{B}, \mathcal{E}, \mathcal{F}\}$ to the “lower”

subset $\{\mathcal{C}, \mathcal{D}, \mathcal{G}, \mathcal{H}\}$ and vice versa. We need to count the number of equator-crossings, starting from the chosen beginning of the orbit and use the parity of this number to determine which of these two subsets is the correct descriptor at any given time.

⁴⁶Segment 2 does not correspond to the choice of the initial (Euler) configuration made in Sec. III E. Rather the latter corresponds to segment 3. Renumbering of particles is straightforward, but it would lead to unnecessary complications in the definition/application of the Jacobi vectors.



Chladni Plate and Clamp

The technique of showing the lines of nodes on vibrating metal plates by strewing sand on them was developed by the German physicist Ernst E. F. Chladni. The first mention of the technique is in his book *Entdeckungen ueber die Theorie des Klanges*, published in 1787. Until the twentieth century the standard method of setting the plates into oscillation was drawing the rosined hairs of a violin bow over the edge of the plate, which was normally clamped at its geometrical center. The clamp for this Chladni plate, which is at Allegheny College, is listed at \$4.00 in the 1860 E. S. Ritchie catalogue. (Notes and photograph by Thomas B. Greenslade, Jr., Kenyon College)